Enhancing oxygen/moisture resistance of quantum dots by short-chain, densely cross-linked silica glass network

IOP Publishing Nanotechnology
Nanotechnology 33 (2022) 465202 (11pp) https://doi.org/10.1088/1361-6528/ac86de

Enhancing oxygen/moisture resistance of quantum dots by short-chain, densely cross-linked silica glass network

Xuan Yang[1], Shuling Zhou[1], Xinfeng Zhang[1], Linyi Xiang[1], Bin Xie[2,*] and Xiaobing Luo[1,*]

[1] School of Energy and Power Engineering, Huazhong University of Science and Technology, Wuhan 430074, People's Republic of China
[2] School of Mechanical Science and Technology, Huazhong University of Science and Technology, Wuhan 430074, People's Republic of China

E-mail: binxie@hust.edu.cn and luoxb@hust.edu.cn

Received 18 June 2022, revised 2 August 2022
Accepted for publication 4 August 2022
Published 30 August 2022

Abstract

Quantum dots (QDs) are facing significant photoluminescence degradation in moisture environment. In QDs-silicone composites, the poor water resistance of silicone matrix makes it easy for water and oxygen molecules to erode QDs. To tackle this issue, we proposed a new QDs protection strategy by introducing short-chain silica precursors onto the QDs' surface, so that a dense silica passivation layer could be formed onto the QDs nanoparticles. Sol-gel method based on 3-aminopropyl triethoxysilane (APTES), 3-mercaptopropyl trimethoxysilane (MPTMS), and 3-mercaptopropyl triethoxysilane (MPTES) were adopted to prepare the uniform and crack-free QDs-silica glass (QD-glass). Because of the crosslinking of short-chain precursors, the formed silica glass possesses 38.6% smaller pore width and 68.6% lower pore volume than silicone, indicating its denser cross-linked network surrounding QDs. After 360 h water immersion, the QDs-glass demonstrated a 6% enhancement in red-light peak intensity, and maintained a stable full width at half maximum (FWHM) and peak wavelength, proving its excellent water-resistant ability. However, the conventional QDs-silicone composites not only showed a decrease of 75.3% in red-light peak intensity, but also a broadened FWHM and a redshifted peak wavelength after water immersion. QDs-glass also showed superior photostability after 132 h exposure to blue light. Red-light peak intensity of QDs-glass remained 87.3% of the initial while that of QDs-silicone decreased to 19.8%. And the intensity of QDs-glass dropped to 62.3% of that under 20 °C after thermal treatment of 160 °C. Besides, under increasing driving currents, the light conversion efficiency drop of QDs-glass is only one fifth that of QDs-silicone. Based on the QDs-glass, the white light-emitting diodes was achieved with a high luminous efficiency of 126.5 lm W^{-1} and a high color rendering index of 95.4. Thus, the newly proposed QD-glass has great significance in guaranteeing the working reliability of QDs-converted devices against moisture and high-power environment.

Keywords: quantum dots, silica glass, densely cross-linked network, high power, stability

(Some figures may appear in colour only in the online journal)

1. Introduction

Quantum dots (QDs), a kind of unique semiconducting nanocrystals, have developed over a long period of time and become one of the most noticed luminous materials in recent years. They are widely used in lighting [1–3], displays [4–6], photovoltaics [7, 8], and sensors [9, 10] owing to their unique characteristics such as wide absorption spectra, high color purity, and tunable emission spectra [11]. However, the sensitivity of QDs towards water and oxygen severely hinders

* Authors to whom any correspondence should be addressed.

their widespread application. Water and oxygen molecules could erode the surface structures of QDs, leading to surface ligand detachment, the subsequent defect states, and even core damage [12–17]. Furtherly, exposure to blue light will accelerate the erosion process, which causes irretrievable damage to QDs in the photoluminescent process [14, 18]. In practice, QDs are usually embedded in silicone matrix which has strong water and oxygen permeability, resulting in significant lifetime shrink of QDs. Thus, it is urgent to promote the working stability of QDs by impeding the permeation and erosion of water and oxygen.

Protective barrier coating is a common and effective solution for above problem [19]. Silica is frequently used in coating for its high optical transparency and water resistance [20–27]. However, the hydrophilic hydroxyl on the surface of silica shell weakens its water-resistant ability [28]. To solve this issue, surface-hydrophobic treatment for silica shell has been proposed [29, 30]. In our previous work, the surface of nanosized SiO_2-coated QDs was furtherly modified with enough methyl groups to be superhydrophobic. The nanocomposite-silicone film showed only 1% drop of PLQY after being immersed in water for fifteen days [30]. Nevertheless, the fabrication of nanosized and superhydrophobic SiO_2-coated QDs requires precise control of the coating reaction and surface modification or it may cause severe aggregation among QDs during the coating process.

At present, inorganic glass has gained much attention due to its high chemical stability and dense structure. The silica glass fabricated by sol-gel method is used for QDs encapsulation for its mild reaction conditions, stable structure, and high compatibility with the surface ligands of QDs [31]. During the fabricating process, silica glass prepared by tetraethoxysilane (TEOS) typically uses ammonia or propylamine as a catalyst [32–34]. However, the alkalinity of the catalyst could damage QDs, and result in a rapid reaction rate which makes the QDs-silica glass easy to crack. These shortcomings significantly limit the application of QDs-glass in practical encapsulation.

To solve this problem, we proposed a new protection strategy based on crosslinking of short-chain silica precursors to achieve a dense buffer layer outside QDs. Besides, by optimizing the reaction dynamics, the crack phenomenon in QDs-glass was eliminated, thus promoting the practical application of QDs-silica glass composites in optoelectronics. The catalyst-free fabrication process was achieved by utilizing 3-mercaptopropyl trimethoxysilane (MPTMS), 3-aminopropyl triethoxysilane (APTES), and QDs capped with 3-mercaptopropyl triethoxysilane (MPTES) as the surface ligand. Textural properties and water, photo, thermal, and high-power stability of QDs-silica glass were investigated. QDs-glass maintained its photoluminescent properties both after being immersed in deionized water for 360 h and being exposed to blue light in air for 132 h. And it also showed excellent stability under high temperatures. When operating under large driving currents, only an extremely low decrease in the light conversion efficiency (LCE) was appeared to QDs-glass. Besides, the investigation of optical performance of QDs-glass converted white light-emitting diodes (QGWLEDs) demonstrated its remarkable performance in white-light illumination.

2. Experimental section

2.1. Materials

MPTMS and APTES were purchased from Aladdin Industrials Corporation. Red light-emitting CdSe/ZnS QDs with a peak wavelength of 632 nm and MPTES as surface ligand were provided by Suzhou Xingshuo Nanotech CO., Ltd. Yellow light-emitting YAG: Ce phosphor with a peak wavelength of 538 nm were provided by Intematix. Two-component silicone was purchased from Dow Corning (SYLGARD 184). High power blue LED modules with a peak wavelength of 450 nm were provided by SkyBright.

2.2. Fabrication of QDs-glass and QDs-silicone

Figure 1 shows the fabrication process of QDs-glass. We fabricated the QDs-glass using sol-gel method. In brief, the Si −OR1 (R1 represents CH_2CH_3 or CH_3) in the precursors (APTES, MPTMS and MPTES) reacts with each other to form Si−O−Si and produces small molecules (methanol and ethanol). The produced small molecules will occupy a volume in the SiO_2 network. During the condensation process of the network, the small molecules volatilize and leave pores in the matrix of QDs-glass [28]. The rate of the reaction depends on the PH value of the mixed solution of APTES, MPTMS and QDs. And the pH value of the solution can be controlled by changing the volume ratio of MPTMS to APTES due to the acidity of MPTMS and the alkalinity of APTES. MPTES is utilized as the surface ligands of CdSe/ZnS QDs for following reasons: (1) thiol in MPTES shows strong binding with ZnS shell, (2) ethoxy in MPTES could connect QDs into SiO_2 network to improve their monodispersity in the silica glass matrix. Considering the similarity to MPTES, MPTMS is also available for the surface ligands. First, 1 ml of MPTMS, 0.15 ml of APTES, and 30 μl of QDs-chloroform solution (10 mg ml^{-1}) were mixed and magnetic stirred under 350 rpm at 40%–50% relative humidity (RH) for 3.5 h in air. At this point, most of the short-chain precursors have been crosslinked into a network. Then, the mixture was vacuum-treated to remove most of the small molecules produced by the hydrolysis reaction of precursors. Finally, the mixture was poured into a Teflon mold with size of 15 mm × 15 mm × 1 mm, and cured for 24 h in air. For QDs-silicone film, 30 μl QDs-chloroform solution and 1.1 g silicone were mixed followed by a vacuum treatment. After that, the mixture was poured into a mold and thermally cured for 5 min at 85 °C.

2.3. Preparation of QGWLEDs

QGWLEDs were prepared in a remote-packaging structure, as shown in figure 2. By utilizing the remote encapsulation structure with QDs-glass on the top layer, the QDs are protected from the high temperature of the chip. First, 0.08 g phosphor were mixed with 1 g silicone followed by a vacuum treatment. Then, the mixture was poured into a blue LED module and cured at 85 °C for 5 min. Finally, QDs-glass was fixed onto the top of the phosphor-filled LED module to prepared the QGWLEDs.

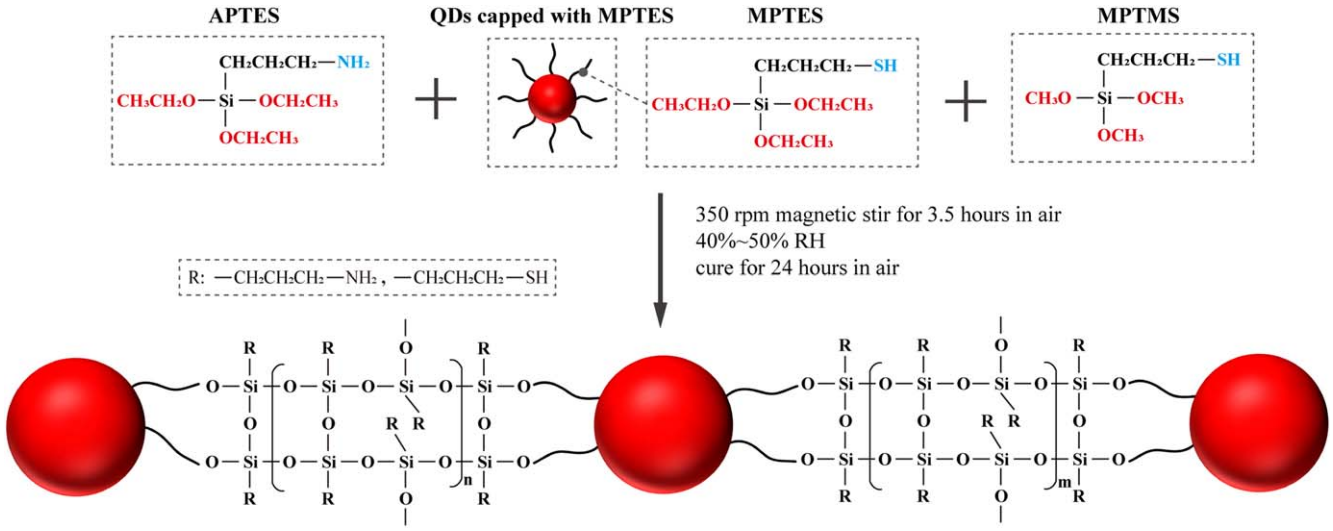

Figure 1. Schematic of the fabrication process of QDs-glass.

2.4. Characterizations

X-ray diffraction (XRD) patterns were collected by a Brucker D8 Advance x-ray diffractometer. Scanning electron microscope (SEM) images and energy-dispersive spectroscopy (EDS) mapping of QDs-glass were measured by a Nova NanoSEM 450, FEI with accelerating voltage of 15 kV. The photoluminescence (PL) spectra were measured by a QuantaMaster 8000 from a xenon lamp at an excitation wavelength of 450 nm. To verify the sol-gel reaction of QDs-glass, Fourier transform infrared spectroscopy (FTIR) images of the samples were measured by a Thermo Nicolet iS50. The textural properties were analyzed through N_2 adsorption and desorption isotherms measured by an ASAP 2020 Accelerated Surface Area and Porosimetry System. The absolute photoluminescence quantum yields (PLQY) were measured by a Hamamatsu Quantaurus-QY from a xenon lamp at an excitation wavelength of 450 nm. The spectra of the QDs-glass and QDs-silicone, excited by a blue light-emitting chip with a peak wavelength of 450 nm and the optical properties of QGWLEDs were tested by an Everfine ATA-1000 Integrating Sphere.

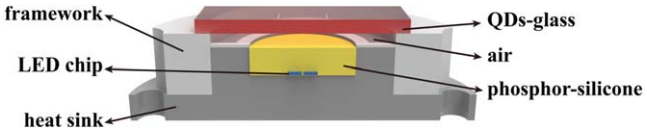

Figure 2. Schematic of the QGWLEDs.

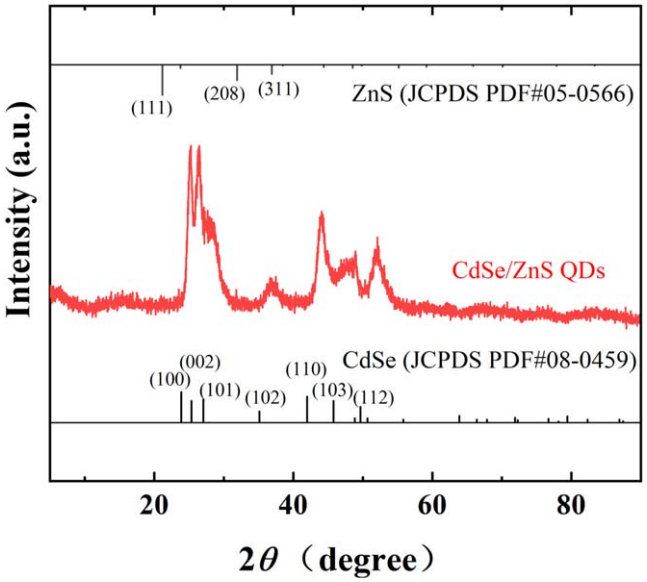

Figure 3. XRD patterns of CdSe/ZnS QDs.

3. Results and discussion

3.1. Characteristics

The crystal structures of the CdSe/ZnS QDs were investigated by XRD as shown in figure 3. The clear diffraction peaks of the QDs can be assigned to cadmoselite CdSe (JCPDS PDF#08-0459) and sphalerite ZnS (JCPSD PDF#05-0566). The diffractions peaks of QDs shifted to higher 2θ angles compared with the PDF card of cadmoselite CdSe and sphalerite ZnS, which was induced from the compressive strain of CdSe core by ZnS shell. Figure 4(a) displays the SEM image of the QDs-glass and the corresponding EDS mapping images. The SEM image demonstrates that there is no crack in QDs-glass. The distribution of Si and Cd elements were clearly showed, confirming the homogenous SiO_2 network and the uniform distribution of QDs in the silica glass matrix, respectively. Figures 4(b) and (c) illustrates the PL spectra of the pristine QDs (QDs-chloroform solution) and QDs-glass. Compared with the pristine QDs, the QDs-glass displays no difference of the peak wavelength, and the full width at half maximum (FWHM) of the QDs-glass is 2 nm narrower. In QDs-glass, the SiO_2 layer formed on the surface of QDs could passivated their defect states, thus decreasing the FWHM [35, 36]. This indicates that the

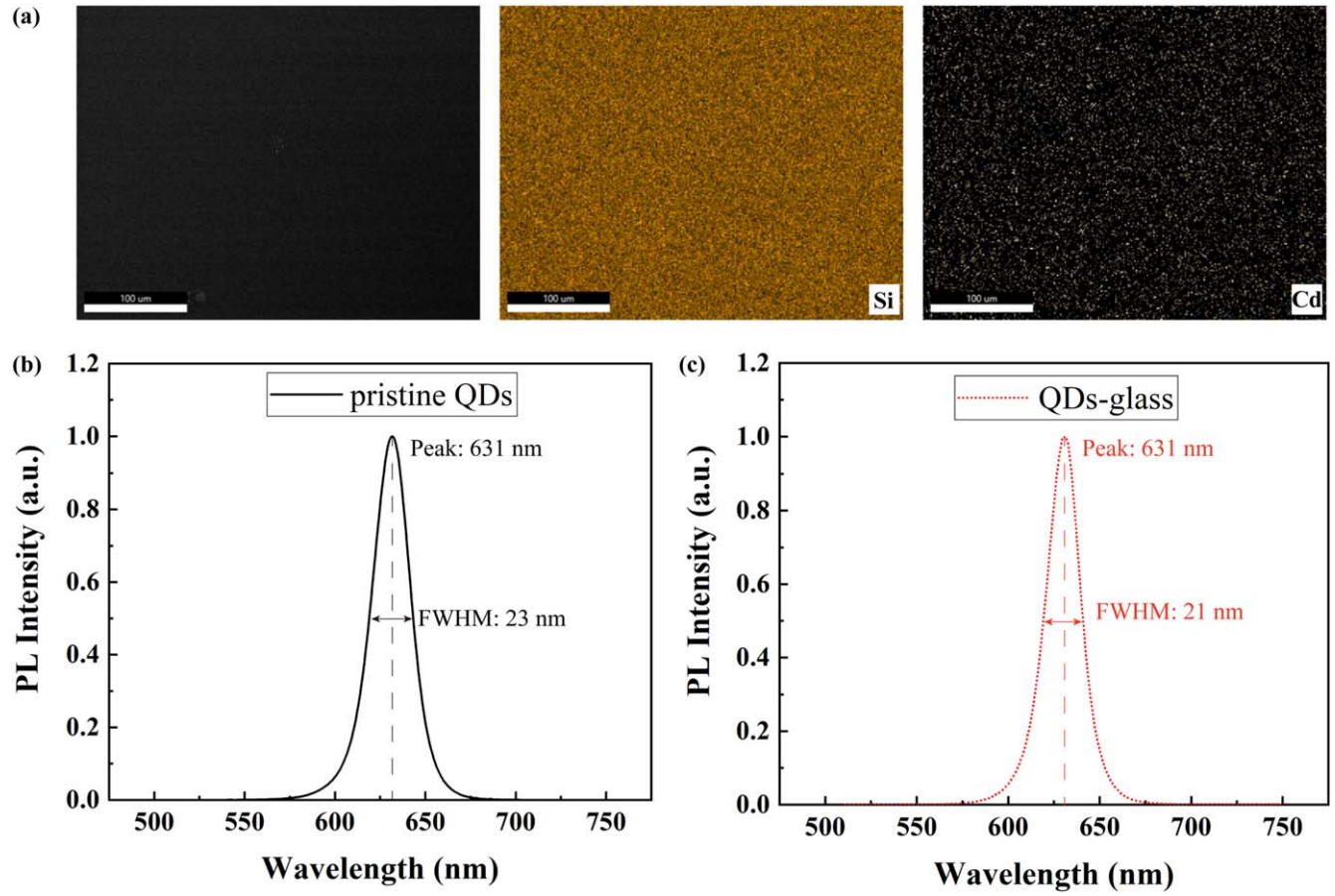

Figure 4. (a) SEM images and the corresponding EDS mapping images of the QDs-glass. Relative PL spectra of (b) pristine QDs and (c) QDs-glass, respectively.

fabrication of QDs-glass has little effect on the photoluminescent performance of the QDs. Figure 5 shows the FTIR spectra of APTES, MPTMS, and silica glass. APTES with amino and MPTMS with thiol could be verified by their unique characteristic peaks of N−H bond at 3374 cm^{-1} and S−H bond at 2564 cm^{-1}, respectively. Through comparison to the precursors, the different variations of C−H bond characteristic peaks of methyl (CH_3) and methylene (CH_2) in QDs-glass could verify the cross-linked reaction between APTES and MPTMS. In detail, there exist absorption peaks at 2973 cm^{-1} and 2883 cm^{-1}, representing the CH_2 and CH_3 of the Si−OCH_2CH_3 in APTES, respectively. The absorption peak at 2839 cm^{-1} represents the CH_3 of the Si−OCH_3 in MPTMS. After reaction, the FTIR spectra of silica glass still has the absorption peaks at 2926 cm^{-1} due to the CH_2 of the reserved aminopropyl (−$(CH_2)_3NH_2$) in APTES and mercaptopropyl (−$(CH_2)_3SH$) in MPTMS. Whereas the absorption peak of CH_3 in silica glass disappeared because of the hydrolytic condensation of ethyoxyl and methoxyl, which proves that APTES and MPTMS have reacted thoroughly and cross-linked to form the dense silica network (Si−O−Si), as illustrated in figure 1.

Figure 6(a) shows the schematic of the cross-linked network of QDs-glass and QDs-silicone. Different from silicone where long chains of molecules are cross-linked into a network, the network of silica glass formed by APTES and

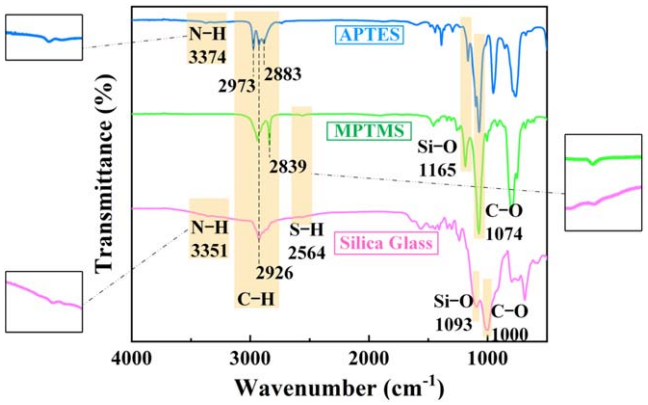

Figure 5. FTIR spectra of APTES, MPTMS, and silica glass.

MPTMS in a highly crossed way is much denser. Theoretically, QDs-glass can efficiently prevent water and oxygen from penetrating into QDs. The textural properties of the as-prepared silica glass and the silicone were investigated by the N_2 adsorption and desorption method at a bath temperature of 77 K. Specific surface area (A_s) was calculated by the Brunauer–Emmett–Teller method. Cumulative pore volume (V_c), average pore width (W_a), and pore width distribution (PWD) were deducted based on the Barrett–Joyner–Halenda method. Table 1 lists the textural properties of the two aforementioned

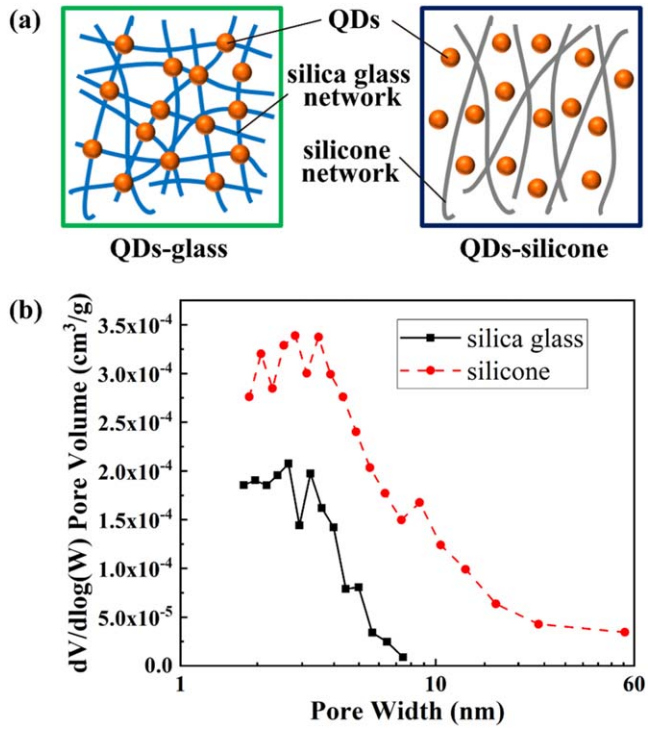

Figure 6. (a) Cross-linked network of QDs-glass and QDs-silicone. (b) PWD of silica glass and silicone.

samples. The average pore width of silica glass is 2.7 nm, which is smaller than 4.4 nm of silicone. In addition, silica glass shows 41.8% lower A_s and 68.6% lower V_c than those of silicone. Furthermore, their significantly different PWD are shown in figure 6(b). It is seen that the pore width of the silicone ranges from 2 nm to 60 nm and shows a much higher pore volume in each width than silica glass. Besides, the range of pore width of silica glass is limited to 1.7–8 nm. The comparison of the textural properties has demonstrated that QDs-glass owns a denser cross-linked network than QDs-silicone, which means that QDs-glass would show a better performance to resist water and oxygen molecules.

3.2. Water stability of QDs-glass and water/oxygen erosion process

As shown in figure 7(a), QDs-glass and QDs-silicone were immersed in deionized water for 360 h to investigate their water stability. Their photoluminescent properties after different immersed time were tested by placing the sample films over a 100 mA current-driven blue light-emitting LED module, as shown in figure 7(b). Figure 7(c) displays the photographs of QDs-glass and QDs-silicone under daylight. QDs-glass shows luster of glass, no crack, and a flat surface. According to the photographs under UV light in figure 7(c), after 360 h of water immersion, QDs-silicone was badly darkened under UV light, but QDs-glass was as bright as before, owing to its denser structure. As the immersed time increased, the relative red-light peak intensity of QDs-glass reached its maximum value at 96 h, which was 111.0% of the initial, and then dropped to 106.0% at 360 h, as shown in figure 8(a). For QDs-silicone, the relative red-light peak intensity continuously dropped during the whole immersion, and finally reduced to 24.7% of the initial intensity. With regards to the red-light power of QDs-glass, defined as the integral of intensity at each red-light emissive wavelength, it almost maintained the same as the red-light peak intensity. However, the red-light power of QDs-silicone kept dropping with a slower speed than its peak intensity and was 41.0% of the initial at 360 h. Besides, the absolute photoluminescence quantum yields (PLQY) of the two samples before and after the water immersion were illustrated in figure 8(b). The initial PLQY of QDs-glass and QDs-silicone are similar, which demonstrates that the fabrication process of QDs-glass barely harmed the QDs. After the immersion, the PLQY of QDs-glass increased by 6.6% while that of QDs-silicone decreased by 15.0%.

Table 1. Textural properties of silica glass and silicone.

Samples	W_a (nm)	A_s ($m^2\ g^{-1}$)	V_c ($cm^3\ g^{-1}$)
Silica glass	2.7	3.81×10^{-1}	0.83×10^{-4}
Silicone	4.4	6.55×10^{-1}	2.64×10^{-4}

It can be concluded from the above results that, the variation of the red-light peak intensity, the red-light power, and the absolute PLQY of QDs-silicone differed a lot between each other but that of QDs-glass stayed similar, as listed in table 2. Detailed discussions on this issue are as follows. The absolute PLQY is defined as the ratio of emitted photon number to absorbed photon number. Thus, the increase or decrease of the PLQY reveals the gain or loss of the emitted photon number on the same absorbed photon number condition during the light conversion process. According to figure 8(b), the emitted red-light photon number of QDs-glass was added by 6.6% while that of QDs-silicone was lost by 15.0%. In addition, as shown in figures 8(c) and (d), the spectra of QDs-glass barely changed, but QDs-silicone faced about 60% drop in intensity, 17 nm broadening in FWHM, and 15 nm redshift in peak wavelength. The broadened FWHM reveals a wider range of emissive wavelengths, which means that the proportion of red-light peak intensity in red-light power was reduced. This explains why the red-light power of QDs-silicone decreased less than the red-light peak intensity. On the other hand, the significant redshift in the spectra of QDs-silicone brought large Stokes energy loss which sharply declined the energy of the red-light photon. Due to the decrease of emitted red-light photon number, the broadened FWHM, and the Stokes energy loss of redshifted photon, the red-light peak intensity of QDs-silicone severely dropped. For QDs-glass, there are no changes of FWHM and peak wavelength in the spectra, but only the increased emitted red-light photon number. In other words, the variation of emitted red-light photon number of QDs-glass decides the red-light peak intensity and the red-light power which both increased by 6%, the same as the enhancement of PLQY.

The underlying mechanisms of above-mentioned photoluminescence phenomena are as follows. The enhancement

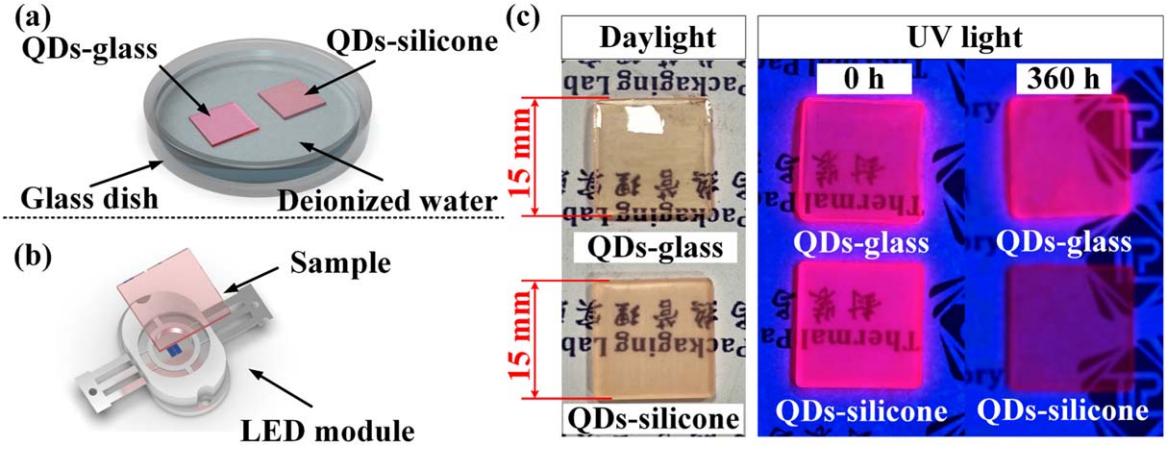

Figure 7. (a) Schematic of the water stability test for QDs-glass and QDs-silicone. (b) Schematic of the photoluminescent properties test device. (c) Photographs of QDs-glass and QDs-silicone under daylight, and under UV light at 0 h and 360 h, respectively.

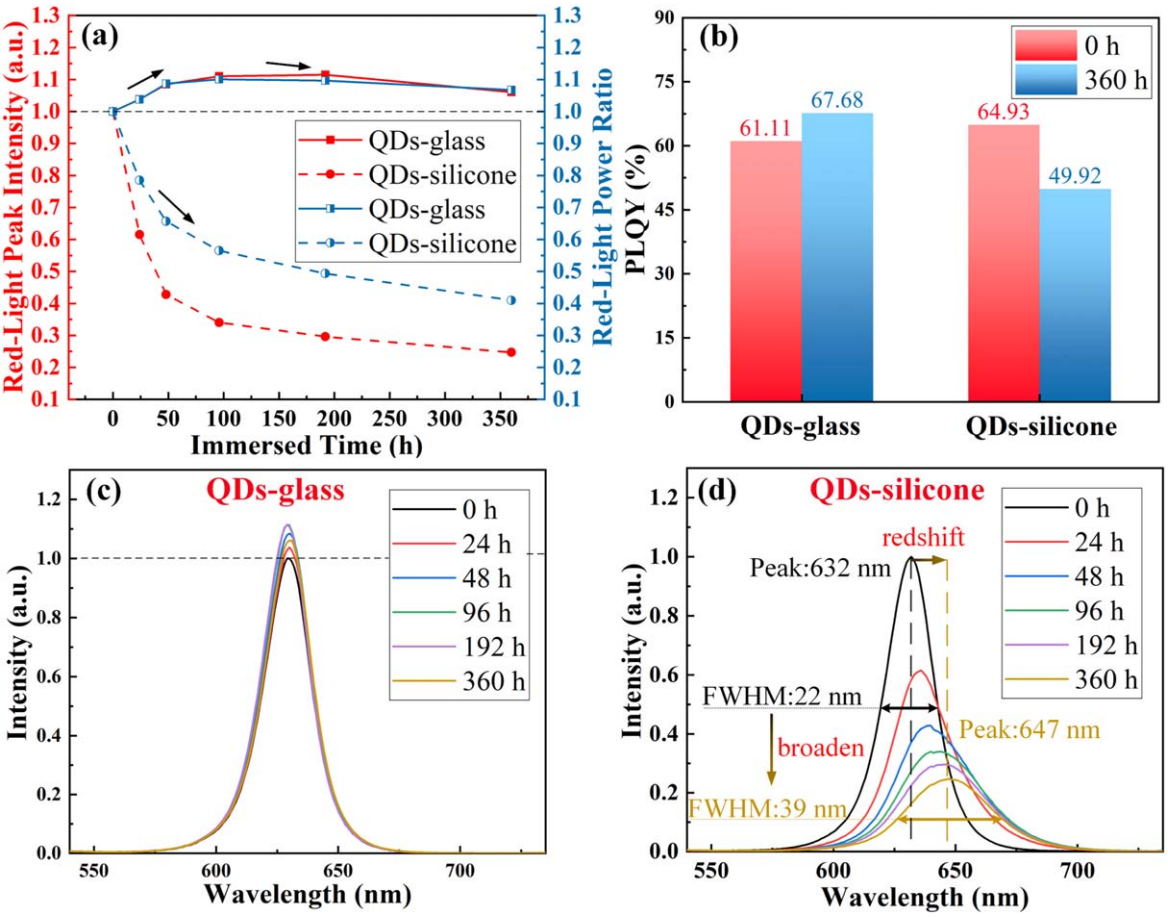

Figure 8. (a) Relative red-light peak intensity and red-light power ratio of QDs-glass and QDs-silicone after different immersed time under a driving current of 100 mA. (b) PLQY of QDs-glass and QDs-silicone before and after being immersed in water for 360 h. Spectra of (c) QDs-glass and (d) QDs-silicone after different immersed time under a driving current of 100 mA, respectively.

Table 2. Variation of the red-light peak intensity, red-light power, and PLQY of QDs-glass and QDs-silicone.

Samples	Red-light peak intensity	Red-light power	PLQY
QDs-glass	+6.0%	+6.7%	+6.6%
QDs-silicone	−75.3%	−59.0%	−15.0%

and deterioration of the photoluminescent properties of the two films were attributed to the diverse structural changes of QDs, after interacting with water and oxygen. QDs consist of core materials, shell materials, and surface ligands, as shown in figure 9(a). The radiative recombination produces photons, and the non-radiative recombination caused by defect states (DS) produces phonons. These two processes reveal the

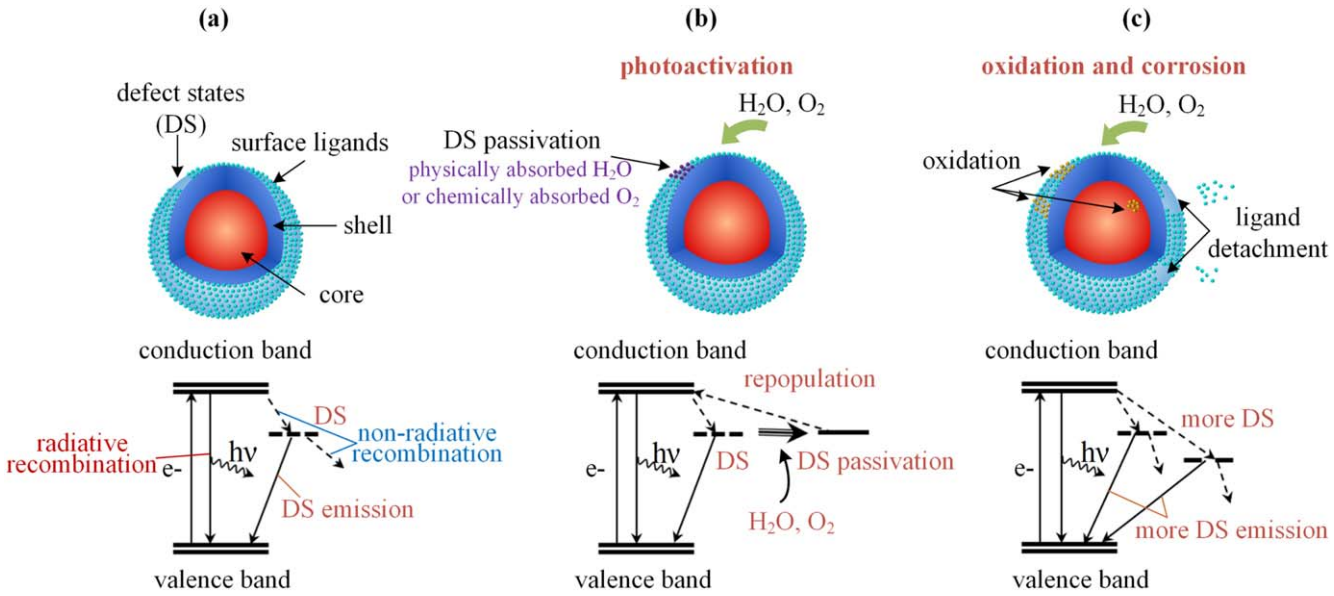

Figure 9. Schematic of (a) quantum dots, (b) the photoactivation process, and (c) oxidation and corrosion process.

photoluminescence and quenching mechanism of QDs [37]. Besides, there is also defect states emission (DS emission) which emits photons with lower energy, causing a broadening in FWHM and a redshift in emissive spectra [18, 38–40].

As shown in figure 9(b), for QDs-glass, after 96 h of water immersion, their photoluminescence was enhanced, which is known as photoactivation. When exposed to moisture, the defect states can physically absorb H_2O and chemically absorb O_2 to form the passivated defect states (DS passivation). The DS passivation can repopulate the electrons from defect states to the conduction band of the QDs, thus increasing the radiative recombination [14, 41, 42]. The drop in the photoluminescence of QDs-glass (96–360 h) and QDs-silicone (0–360 h) is caused by the oxidation and corrosion from H_2O and O_2, as shown in figure 9(c). Water and oxygen molecules eroded the surface of QDs, thus leading to ligand detachment and shell oxidization. The detachment of surface ligand and the oxidation of the QDs induced new defect states, and brought numerous non-radiative recombination which severely damaged the photoluminescent properties of QDs.

The differences in matrix network density between QDs-glass and QDs-silicone led to the disparity of their photoluminescent properties after the water immersion. Owing to the dense network of QDs-glass, the concentration of water and oxygen around the QDs in the matrix was relatively low, which led to minor interactions between QDs and water and oxygen molecules. Thus, the photoactivation process could be maintained for a long period of 96 h in the water immersion of QDs-glass. At the same time, the oxidation and corrosion effect on the QDs was so weak that the defect states were formed extremely slowly. As a result, the intensity of the QDs after the immersion was still higher than the initial. However, due to the loose network of QDs-silicone, water and oxygen rapidly intruded into the matrix and violently reacted with QDs producing a large number of defect states. The numerous defect states, accompanied by lots of surface DS emission, significantly weakened the photoluminescent properties of QDs with a broadened FWHM and redshifted peak wavelength, as illustrated in figure 8(d). In addition, it is worth mentioning that the photoactivation process of the QDs-silicone was not able to be monitored, because the degradation from a huge number of defect states was so strong to cover up the enhancement from the DS passivation.

3.3. Photostability and thermal stability of QDs-glass

The photostability of the QDs-glass and QDs-silicone were tested by exposing the samples to a 0.3 W blue LED chip in air. The photoluminescent properties of the samples were tested every 12 h under a driving current of 60 mA. The red-light peak intensity of QDs-glass increased during the first 12 h and achieved its maximum of 109.1% of the initial intensity, and then dropped to 87.3% at 132 h as shown in figure 10(a). However, the red-light peak intensity of QDs-silicone continuously dropped during the whole test and end up with an intensity of 19.8% of the initial. When exposed to blue light in air, the water and oxygen molecules in air can erode the QDs and bring structural changes, which produces defect states and results in the variation in photoluminescent properties. This phenomenon is similar to that of the samples in water immersion. The photo-aging QDs-glass showed a photoactivation during the initial period of time (0–12 h) and then went through a corrosion and oxidation (12–132 h) when exposed to blue light. And for QDs-silicone, corrosion and oxidation of the QDs dominated the whole photo-aging test (0–132 h). The difference between water immersion process and blue-light exposure process is that because of the illumination of blue light, the erosion of water and oxygen to QDs was accelerated. Therefore, the photoluminescent properties of QDs varied more rapidly both in QDs-glass and QDs-silicone. Thanks to the denser structure to resist the

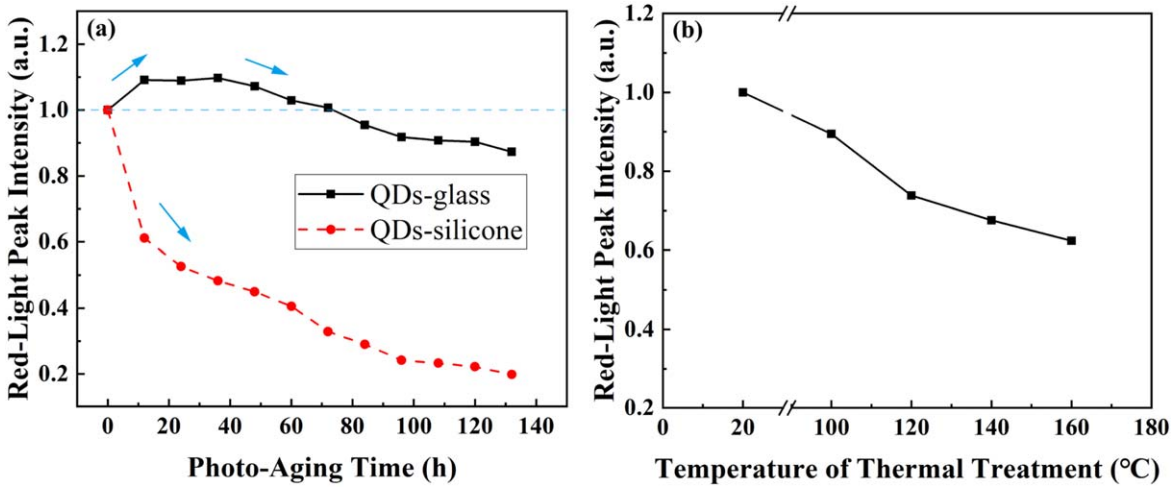

Figure 10. (a) Relative red-light peak intensity of QDs-glass and QDs-silicone after different immersed time under a driving current of 60 mA. (b) Relative red-light peak intensity of QDs-glass after thermal treatments under different temperatures.

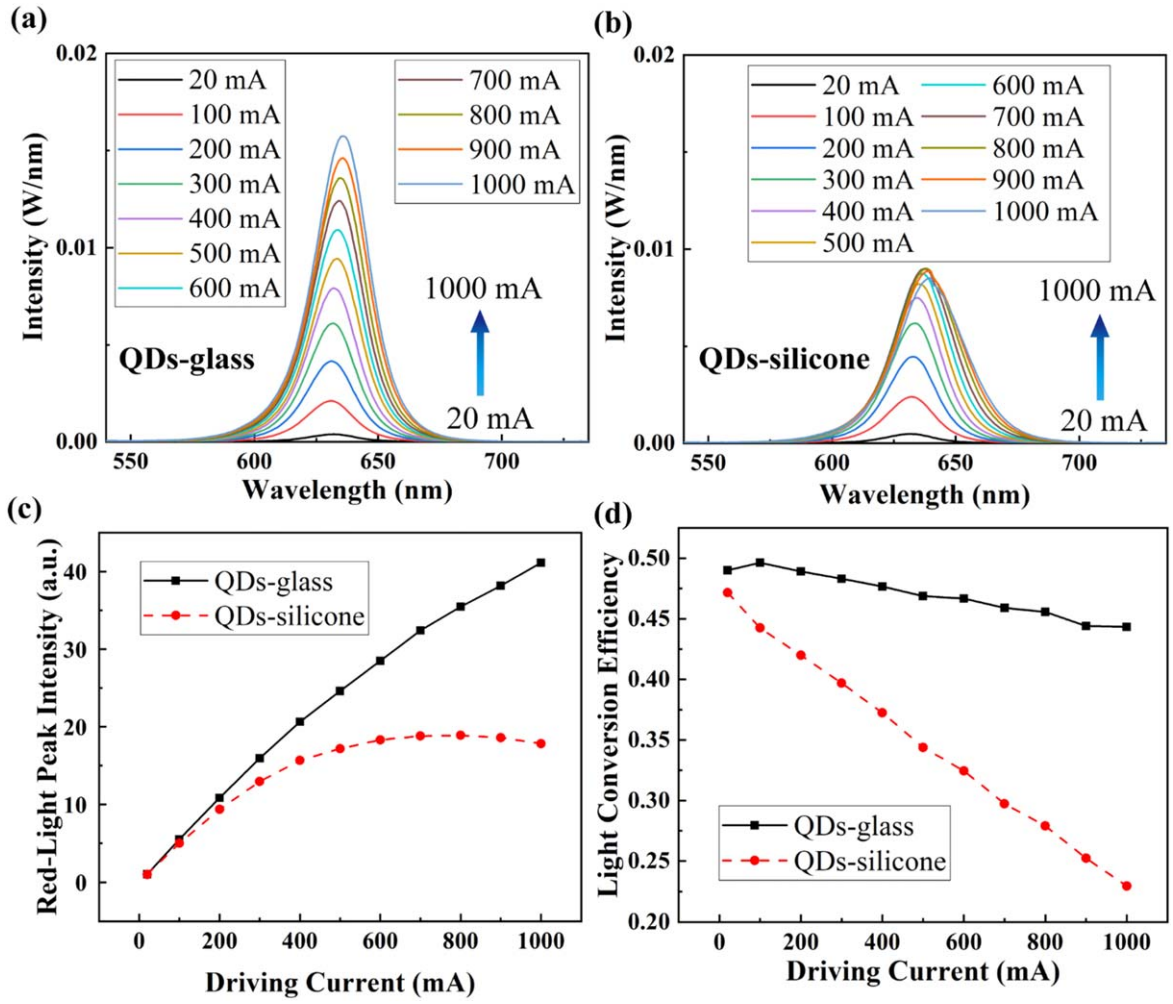

Figure 11. Spectra under increasing driving currents of (a) QDs-glass and (b) QDs-silicone, respectively. (c) Red-light peak intensity and (d) LCE under increasing driving currents of QDs-glass and QDs-silicone, respectively.

water and oxygen molecules, the QDs-glass showed superior photostability than QDs-silicone under the blue light.

The thermal stability of the QDs-glass was also investigated. QDs-glass was thermal treated in an oven under different temperature of 100 °C, 120 °C, 140 °C and 160 °C for 0.5 h. Then the sample was cooled in air for another 0.5 h. Finally, the red-light peak intensity of thermal-treated QDs-glass was tested under a driving current of 60 mA.

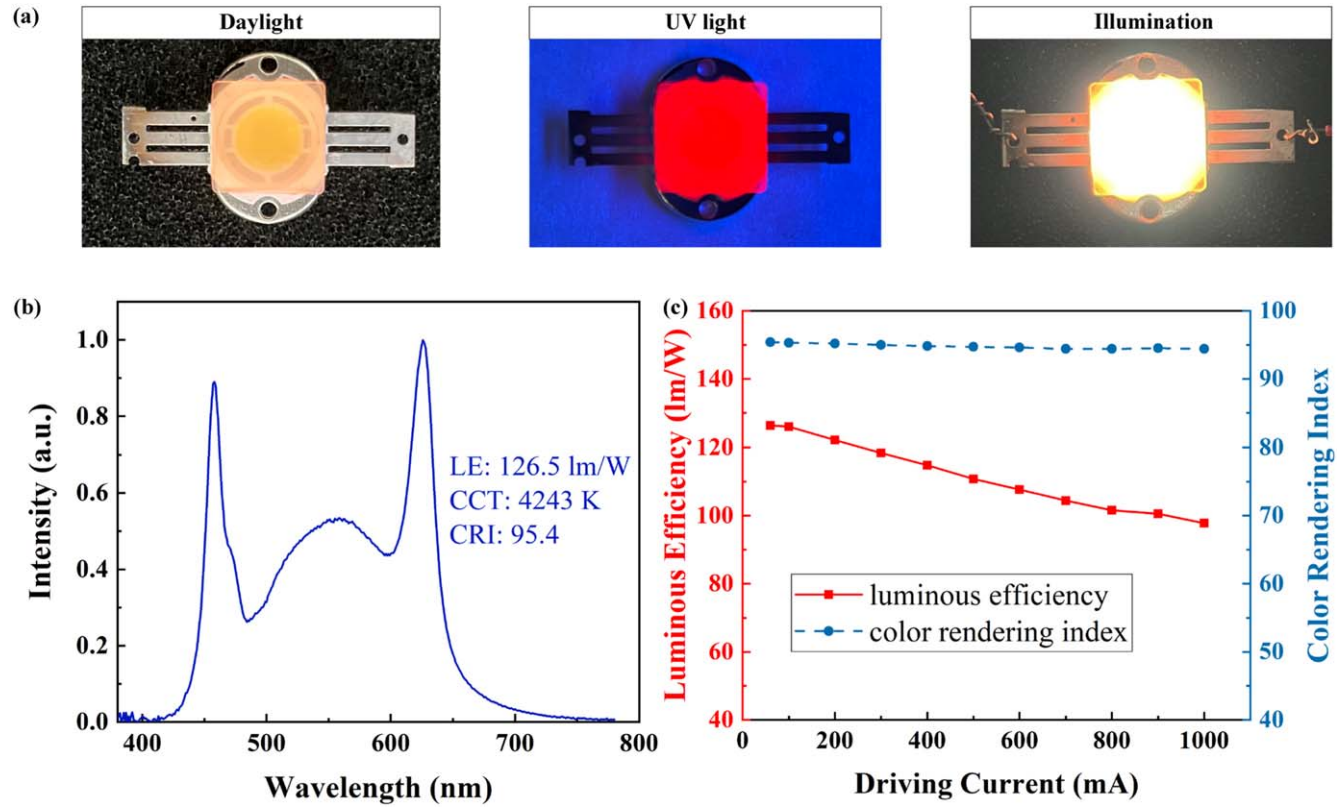

Figure 12. (a) Photographs of QGWLEDs under daylight, under UV light and with illumination. (b) Spectra and optical properties of QGWLEDs under driving current of 60 mA. (c) LE and CRI of QGWLEDs under increasing driving currents.

Figure 10(b) illustrates the relative red-light peak intensity of QDs-glass under different temperature of thermal treatment. As the temperature increased, the red-light peak intensity of QDs-glass dropped. This is because high temperature can bring structural changes to QDs and generated defect states, which severely damages the photoluminescent properties of QDs [43]. For QDs-glass, its intensity remained 89.4%, 73.9%, 67.5% and 62.3% under 100 °C, 120 °C, 140 °C and 160 °C of that under 20 °C respectively, showing an outstanding stability against the high temperature.

3.4. High-power stability of QDs-glass

Optical performance under increasing driving currents from 20 mA to 1000 mA were also investigated. Figures 11(a) and (b) display the emissive spectra of QDs-glass and QDs-silicone under increasing driving currents, respectively. The intensity of QDs-glass increased almost linearly with the increasing driving currents, but the increased magnitude of the intensity of QDs-silicone decreased sharply, as shown in figure 11(c). LCE is the ratio of the emitted red-light power to the absorbed blue-light power by QDs, as shown in figure 11(d). As the driving currents increased, the LCE of QDs-glass only showed a small decrease of 9.5% but that of QDs-silicone sharply decreased by 51.3%. This discrepancy was mainly due to the different dispersion of QDs in silicone and silica glass. The MPTES ligands of QDs have a highly similar chemical composition to the glass matrix formed by APTES and MPTMS. It has been proved that the similarity between capped ligands of QDs and matrix polymers can effectively avoid the attraction and agglomeration among the nanoparticles, improving the dispersion of the particles within the matrix [44, 45]. Therefore, as the driving currents increased, the LCE of QDs-glass showed ultrahigh stability. The silicone matrix contains polymer chains with high molecular weight, for example, polydimethylsiloxane. And the common capped ligands of QDs such as oleic acid and the MPTES in this work both show a significant chemical difference to the silicone matrix. In this situation, the QDs are more inclined to aggregate [46]. On this basis, under the increasing driving currents, the optical density is raised followed by an extremely increased probability that the QDs reabsorbed light. As a result, the LCE of QDs-silicone decreased severely due to the strongly enhanced reabsorption effect.

3.5. Optical performance of QGWLEDs

Figure 12(a) provides the photographs of QGWLEDs under daylight, under UV light, and with illumination. QDs-glass is fixed on the top of a blue LED module. The luminous QGWLEDs emits high-quality white light and its spectra is shown in figure 12(b). Under a driving current of 60 mA, QGWLEDs shows high luminous efficiency (LE) of 126. 5 lm W^{-1}, correlated color temperature of 4243 K, and high color rendering index (CRI) of 95.4, indicating its

superior optical performance. Figure 12(c) illustrates LE and CRI variation under increasing driving currents from 60 to 1000 mA. The LE dropped with the increasing driving currents, but the CRI of QGWLEDs remained stable which revealed the consistent color rendering ability under various lighting conditions. The above discussion demonstrated that QGWLEDs owned remarkable performance in high quality white-light illumination.

4. Conclusion

Oxidation corrosion from water and oxygen will cause the photoluminescent degradation of QDs and the lifetime shrinks of QDs-converted luminescent devices. To protect QDs from the erosion of water and oxygen, we proposed a new protection strategy by crosslinking short-chain silica precursors to achieve a surface buffer layer outside QDs. And the crack-free QDs-glass was fabricated by utilizing MPTMS, APTES, and QDs capped with MPTES as the surface ligand without any catalysts. The uniform QDs-glass was proved to have the densely cross-linked network with small pore width of 2.7 nm and low pore volume of 0.83×10^{-4} cm^3 g^{-1}. Owing to the dense structure, the photoluminescent intensity and spectra of QDs-glass were able to be nearly maintained after being immersed in deionized water for 360 h. In a contrast, QDs-silicone with poor water resistance showed a decrease of 75.3% in red-light peak intensity, 17 nm broadening in FWHM, and 15 nm redshift in peak wavelength. The dense structure also contributed to the stable performance of QDs-glass when it was exposed to blue light for 132 h. In red-light peak intensity, QDs-glass remained 87.3% of the initial intensity while that of QDs-silicone decreased to 19.8%. And after several thermal treatments of different temperatures, QDs-glass shows an excellent stability. In addition, due to the high dispersity of QDs in silica glass, the LCE of QDs-glass only decreased by 9.5% with the increasing driving currents but 51.3% for QDs-silicone. The prepared QGWLEDs showed a high LE of 126.5 lm W^{-1} and a high CRI of 95.4, indicating its remarkable performance in high quality white-light illumination. The dense network and high dispersity of QDs-glass have enhanced the stability of QDs towards moisture and high-power excitation which furtherly promotes the wider application of QDs devices.

Acknowledgments

This work is supported by the National Natural Science Foundation of China (51625601, 52106089).

Data availability statement

All data that support the findings of this study are included within the article (and any supplementary files).

ORCID iDs

Xiaobing Luo https://orcid.org/0000-0002-6423-9868

References

[1] He H, Mei S, Wen Z, Yang D, Yang B, Zhang W, Xie F, Xing G and Guo R 2022 Recent advances in blue perovskite quantum dots for light-emitting diodes *Small* **18** 2103527
[2] Kalsoom U, Yi R, Qu J and Liu L 2021 Nonlinear optical properties of CdSe and CdTe core–shell quantum dots and their applications *Front. Phys.* **9** 612070
[3] Shang Y and Ning Z 2017 Colloidal quantum-dots surface and device structure engineering for high-performance light-emitting diodes *Natl Sci. Rev.* **4** 170–83
[4] Kang C, Prodanov M, Gao Y, Mallem K, Yuan Z, Vashchenko V and Srivastava A 2021 Quantum-rod on-chip LEDs for display backlights with efficacy of 149 lm W^{-1}: a step toward 200 lm W^{-1} *Adv. Mater.* **33** 2104685
[5] Yang J, Choi M, Yang U, Kim S, Kim Y, Kim J, Kim D and Hyeon T 2021 Toward full-color electroluminescent quantum dot displays *Nano Lett.* **21** 26–33
[6] Yu M, Saeed M, Zhang S, Wei H, Gao Y, Zou C, Zhang L and Yang H 2021 Luminescence enhancement, encapsulation, and patterning of quantum dots toward display applications *Adv. Funct. Mater.* **32** 2109472
[7] Kumar P, Dua S, Kaur R, Kumar M and Bhatt G 2022 A review on advancements in carbon quantum dots and their application in photovoltaics *RSC Adv.* **12** 4714–59
[8] Xu L, Yuan S, Ma L, Zhang B, Fang T, Li X and Song J 2021 All-inorganic perovskite quantum dots as light-harvesting, interfacial, and light-converting layers toward solar cells *J. Mater. Chem. A* **9** 18947–73
[9] Diaz-Alvarez M and Martin-Esteban A 2021 Molecularly imprinted polymer-quantum dot materials in optical sensors: an overview of their synthesis and applications *Biosensors* **11** 79
[10] Galstyan V 2021 Quantum dots: perspectives in next-generation chemical gas sensors a reviews *Anal. Chim. Acta* **1152** 238192
[11] Xie B, Hu R and Luo X 2016 Quantum dots-converted light-emitting diodes packaging for lighting and display: status and perspectives *J. Electron. Packag.* **138** 020803
[12] Amelia M, Avellini T, Monaco S, Impellizzeri S, Yildiz I, Raymo F and Credi A 2011 Redox properties of CdSe and CdSe-ZnS quantum dots in solution *Pure Appl. Chem.* **83** 1–8
[13] Naghadeh S, Luo B, Abdelmageed G, Pu Y, Zhang C and Zhang J 2018 Photophysical properties and improved stability of organic-inorganic perovskite by surface passivation *J. Phys. Chem. C* **122** 15799–818
[14] Moon H, Lee C, Lee W, Kim J and Chae H 2019 Stability of quantum dots, quantum dot films, and quantum dot light-emitting diodes for display applications *Adv. Mater.* **31** 1804294
[15] Paydary P and Larese-Casanova P 2020 Water chemistry influences on long-term dissolution kinetics of CdSe/ZnS quantum dots *J. Environ. Sci.* **90** 216–33
[16] Raja S, Bekenstein Y, Koc M, Fischer S, Zhang D, Lin L, Ritchi R, Yang P and Alivisatos A 2016 Encapsulation of perovskite nanocrystals into macroscale polymer matrices: enhanced stability and polarization *ACS Appl. Mater. Interface* **8** 35523–33
[17] Hu Z, Shu Y, Qin H, Hu X and Peng X 2021 Water effects on colloidal semiconductor nanocrystals: correlation of

photophysics and photochemistry *J. Am. Chem. Soc.* **143** 18721–32
[18] Huang S, Li Z, Wang B, Zhu N, Zhang C, Kong L, Zhang Q, Shan A and Li L 2017 Morphology evolution and degradation of $CsPbBr_3$ nanocrystals under blue light-emitting diode illumination *ACS Appl. Mater. Interfaces* **9** 7249–58
[19] Ji Y, Wang M, Yang Z, Qiu H, Ji S, Dou J and Gaponenko N 2020 Highly stable Na: CsPb(Br, I)(3)@Al_2O_3 nanocomposites prepared by a pre-protection strategy *Nanoscale* **12** 6403–10
[20] Goryacheva O, Wegner K, Sobolev A, Hausler I, Gaponik N, Goryacheva I and Resch-Genger U 2022 Influence of particle architecture on the photoluminescence properties of silica-coated CdSe Core/Shell quantum dots *Anal. Bioanal. Chem.* **414** 4427–39
[21] Kim Y, Lee H, Kang S and Bae B 2019 Two-step-enhanced stability of quantum dots via silica and siloxane encapsulation for the long-term operation of light-emitting diodes *ACS Appl. Mater. Interfaces* **11** 22801–8
[22] Li H, Wu K, Lim J, Song H and Klimov V 2016 Doctor-blade deposition of quantum dots onto standard window glass for low-loss large-area luminescent solar concentrators *Nat. Energy* **1** 16157
[23] Liu Y, Zhang L, Long X, Jiang P, Geng C and Xu S 2021 Ultra-stable $CsPbBr_3$ nanocrystals with lead-carboxylate/SiO_2 encapsulation for LED applications *J. Mater. Chem. C* **9** 12581–9
[24] Liu Z, Li F, Huang G, Zhao F, Zhang W, Jiang G, Cheng S, Fang Z, Zhu Q and Huang Y 2021 Stability improvement of photoluminescent QLEDs based on Mn-doped all-inorganic metal halide perovskite quantum dots with silica shell *J. Alloys Compd.* **888** 161505
[25] Sun C, Zhang Y, Ruan C, Yin C, Wang X, Wang Y and Yu W 2016 Efficient and stable white LEDs with silica-coated inorganic perovskite quantum dots *Adv. Mater.* **28** 10088–94
[26] Wang B, Zhang S, Liu B, Li J, Cao B and Liu Z 2020 Stable $CsPbBr_3$: Sn@SiO_2 and Cs_4PbBr_6: Sn@SiO_2 core–shell quantum dots with tunable color emission for light-emitting diodes *ACS Appl. Nano Mater.* **3** 3019–27
[27] Zhang L, Xie Y, Tian Z, Liu Y, Geng C and Xu S 2021 Thermal conductive encapsulation enables stable high-power perovskite-converted light-emitting diodes *ACS Appl. Mater. Interfaces* **13** 30076–85
[28] Ciriminna R, Fidalgo A, Pandarus V, Beland F, Ilharco L and Pagliaro M 2013 The sol-gel route to advanced silica-based materials and recent applications *Chem. Rev.* **113** 6592–620
[29] Tu S, Yin Q, Shang B, Chen M and Wu L 2019 Stable perovskite quantum dots coated with superhydrophobic organosilica shells for white light-emitting diodes *Chem.—Asian J.* **14** 3830–4
[30] Zhou S, Xie B, Yang X, Zhang X and Luo X 2022 Superior hydrophobic silica-coated quantum dot for stable optical performance in humid environments *Nanotechnology* **33** 195202
[31] Xia M, Luo J, Chen C, Liu H and Tang J 2019 Semiconductor quantum dots-embedded inorganic glasses: fabrication, luminescent properties, and potential applications *Adv. Opt. Mater.* **7** 1900851
[32] Wang Q, Iancu N and Seo D 2005 Preparation of large transparent silica monoliths with embedded photoluminescent CdSe@ZnS core/shell quantum dots *Chem. Mater.* **17** 4762–4
[33] Shinae J, Lee J and Jang E 2013 Highly luminescent and photostable quantum dot-silica monolith and its application to light-emitting diodes *ACS Nano* **7** 1472–7
[34] Sun C, Shen X, Zhang Y, Wang Y, Chen X, Ji C, Shen H, Shi H, Wang Y and Yu W 2017 Highly luminescent, stable, transparent and flexible perovskite quantum dot gels towards light-emitting diodes *Nanotechnology* **28** 365601
[35] Wang S, Li C, Yang P, Ando M and Murase N 2012 Silica encapsulation of highly luminescent hydrophobic quantum dots by two-step microemulsion method *Colloids Surf. A* **395** 24–31
[36] Su M, Wu D, Fan B, Wang F, Wang K and Luo Z 2018 Synthesis of highly efficient and stable $CH_3NH_3PbBr_3$ perovskite nanocrystals within mesoporous silica through excess CH_3NH_3Br method *Dyes Pigm.* **155** 23–9
[37] Kaur G and Tripathi S 2014 Probing photoluminescence dynamics of colloidal CdSe/ZnS Core/Shell nanoparticles *J. Lumin.* **155** 330–7
[38] Guleroglu G and Unlu C 2021 Spectroscopic investigation of defect-state emission in CdSe quantum dots *Turk. J. Chem.* **45** 520–7
[39] Samuel B, Mathew S, Anand V, Correya A, NampooriV and Mujeeb A 2018 Surface defect assisted broad spectra emission from cdse quantum dots for white LED application *Mater. Res. Express* **5** 025009
[40] Yang Z, Wen Y, Meng Q, Liu Y, Song Y, He X, Li A, Yu G, Yang Y and Wu W 2010 Impact of noble metal nanostructures on surface trapping state of semiconductor quantum dots *Appl. Phys. Lett.* **96** 043118
[41] Pechstedt K, Whittle T, Baumberg J and Melvin T 2010 Photoluminescence of colloidal CdSe/ZnS quantum dots: the critical effect of water molecules *J. Phys. Chem. C* **144** 12069–77
[42] Jones M, Nedeljkovic J, Ellingson R, Nozik A and Rumbles G 2003 Photoenhancement of luminescence in colloidal CdSe quantum dot solutions *J. Phys. Chem. B* **107** 11346–52
[43] Zhao Y, Riemersma C, Pietra F, Koole R, Donega C and Meijerink A 2012 High-Temperature luminescence quenching of colloidal quantum dots *ACS Nano* **6** 9058–67
[44] Tao P, Li Y, Siegel R and Schadler L 2013 Transparent luminescent silicone nanocomposites filled with bimodal PDMS-brush-grafted CdSe quantum dots *J. Mater. Chem. C* **1** 86–94
[45] Akcora P *et al* 2009 Anisotropic Self-assembly of spherical polymer-grafted nanoparticles *Nat. Mater.* **8** 354–9
[46] Li Z, Li J, Deng Z, Liang J and Li J 2021 Unraveling the origin of low optical efficiency for quantum dot white light-emitting diodes from the perspective of aggregation-induced scattering effect *IEEE Trans. Electron Devices* **68** 1738–45